Monthly Notices
of the
ROYAL ASTRONOMICAL SOCIETY

MNRAS **471,** 4286–4299 (2017)
Advance Access publication 2017 July 14

doi:10.1093/mnras/stx1755

Jetted tidal disruptions of stars as a flag of intermediate mass black holes at high redshifts

Anastasia Fialkov★ and Abraham Loeb

Institute for Theory and Computation, Harvard University, 60 Garden Street, Cambridge, MA 02138, USA

Accepted 2017 July 11. Received 2017 June 30; in original form 2016 November 1

ABSTRACT

Tidal disruption events (TDEs) of stars by single or binary supermassive black holes (SMBHs) brighten galactic nuclei and reveal a population of otherwise dormant black holes. Adopting event rates from the literature, we aim to establish general trends in the redshift evolution of the TDE number counts and their observable signals. We pay particular attention to (i) jetted TDEs whose luminosity is boosted by relativistic beaming and (ii) TDEs around binary black holes. We show that the brightest (jetted) TDEs are expected to be produced by massive black hole binaries if the occupancy of intermediate mass black holes (IMBHs) in low-mass galaxies is high. The same binary population will also provide gravitational wave sources for the evolved Laser Interferometer Space Antenna. In addition, we find that the shape of the X-ray luminosity function of TDEs strongly depends on the occupancy of IMBHs and could be used to constrain scenarios of SMBH formation. Finally, we make predictions for the expected number of TDEs observed by future X-ray telescopes finding that a 50 times more sensitive instrument than the Burst Alert Telescope (BAT) on board the *Swift* satellite is expected to trigger ∼10 times more events than BAT, while 6–20 TDEs are expected in each deep field observed by a telescope 50 times more sensitive than the *Chandra X-ray Observatory* if the occupation fraction of IMBHs is high. Because of their long decay times, high-redshift TDEs can be mistaken for fixed point sources in deep field surveys and targeted observations of the same deep field with year-long intervals could reveal TDEs.

Key words: galaxies: jets – cosmology: theory – X-rays: bursts.

1 INTRODUCTION

Supermassive black holes (SMBHs) with masses between 10^6 and $10^{10}\,M_\odot$ (Kormendy & Richstone 1995; Magorrian et al. 1998; Gultekin et al. 2009; Ghisellini et al. 2010; Thomas et al. 2016) are observed to reside at the centres of dark matter haloes with masses $\gtrsim 10^{12}\,M_\odot$. Smaller dark matter haloes, such as hosts of present-day dwarf galaxies or galaxies at high redshifts, are expected to be populated with intermediate mass black holes (IMBHs) with masses in the range $\sim 10^2$–$10^6\,M_\odot$ (Greene 2012). The origin of SMBHs and IMBHs is still not well understood. In hierarchical structure formation, these black holes are expected to grow from initial seeds as a result of galaxy mergers in which black holes coalesce (see Graham 2016, for review). In this picture, gas-rich mergers fuel active galactic nuclei (AGNs) emitting energy in the optical, ultraviolet and X-ray bands. [It should be noted that major mergers are not the only process through which luminous AGNs could form. In particular, by analysing a sample of 20 optically and X-ray selected luminous AGNs at $z \sim 0.6$, Villforth et al. (2017) concluded that other processes such as minor mergers and secular processes dominate AGN formation.] Roughly 10 per cent of AGNs at $z \lesssim 5$ are radio-loud (Jiang et al. 2007), producing a pair of collimated relativistic jets that could be observed to greater distances because of the relativistic beaming effect. The fraction of radio-loud quasars at higher redshifts ($z \sim 6$) was shown to be $8^{+5.0}_{-3.2}$ per cent (Bañados et al. 2015), suggesting no evolution of the radio-loud fraction with z (note, however, that Jiang et al. 2007, found stronger redshift evolution with redshift). On the other hand, if the merger is dry and the merging galaxies do not have enough gas to feed the black hole, a dormant massive black hole (MBH) results without observable electromagnetic signature.

Even though the samples of both SMBHs and IMBHs build up, the percentage of galaxies hosting central black holes (the so-called occupation fraction) is still unclear, especially in low-mass galaxies (Greene & Ho 2007), and until recently IMBHs were considered hypothetical. However, recent observations have shown that some of dwarf galaxies in the local Universe could indeed be populated by IMBHs (Farrell et al. 2009; Reines et al. 2013; Moran et al. 2014; Baldassare et al. 2015, 2017). The growing observational evidence includes 151 dwarf galaxies with candidate black holes in the mass range 10^5–$10^6\,M_\odot$ as identified from optical emission line ratios and/or broad Hα emission (Reines et al. 2013); 28 AGNs with black hole masses in the 10^3–$10^4\,M_\odot$ range in nearby low-mass,

★ E-mail: anastasia.fialkov@cfa.harvard.edu

low-luminosity dwarf galaxies were found with the Sloan Digital Sky Survey (Moran et al. 2014). In addition, Lemons et al. (2015) showed that large fraction of hard X-ray sources in dwarf galaxies are ultraluminous, suggesting that they actually are IMBHs; Yuan et al. (2014) describe four dwarf Seyferts with masses $<10^6\,M_\odot$; Baldassare et al. (2015) reported observations of a $5\times10^4\,M_\odot$ black hole in the dwarf galaxy RGG 118; while Baldassare et al. (2017) list 11 additional black holes with masses between 7×10^4 and $1\times10^6\,M_\odot$. Finally, it was shown that more than 20 per cent of early-type galaxies with a stellar mass less than $10^{10}\,M_\odot$ are expected to have MBHs in their cores (Miller et al. 2015). All these observational evidence suggest that IMBHs in dwarf galaxies are not as exotic as previously thought.

One way to improve our constraints on the black hole occupation fraction is by probing the population of quiescent black holes when they are temporary illuminated by a tidal disruption event (TDE) in which a star passing too close to the black hole is shredded by a gravitational tide that exceeds the self-gravity of the star. Theoretical work on TDEs spans several decades, including works by Hill (1975), Frank & Rees (1976), Lacy, Townes & Hollenbach (2011), Carter & Luminet (1983), Rees (1988), Evans & Kochaneck (1989), Phinney (1989), Magorrian & Tremaine (1999), Wang & Merritt (2004), Perets, Hopman & Alexander (2006), Guillochon & Ramirez-Ruiz (2013), Stone, Sari & Loeb (2013), Stone & Metzger (2016), Roth et al. (2016) and others. When a TDE occurs, part of the stellar mass is ejected away, forming an elongated stream and heating the ambient medium (Guillochon & McCourt 2017), while the bound debris are accreted by the black hole emitting bright observable flare at a wide range of wavelengths from radio to γ-rays (Rees 1990). However, for very MBHs ($3\times10^8\,M_\odot$ for a solar mass star) the tidal disruption distance is smaller than the Schwarzschild radius and stars are swallowed whole without exhibiting TDE flares. The emission peaks in the UV or soft X-rays with typical peak luminosity in the soft X-rays band being $L_X\sim10^{42}$–$10^{44}\,\mathrm{erg\,s^{-1}}$. The flare decays on the time-scale of months or years as a power law with a typical index $-5/3$, which is often considered to be the telltale signature of a tidal disruption of a star by an MBH.

Following the first detection by *ROSAT* (Komossa & Bade 1999; Bade, Komossa & Dahlem 2016), about 50 TDEs have been observed (Komossa 2015) in hard X-ray (Bloom et al. 2011; Burrows et al. 2011; Cenko et al. 2012; Pasham et al. 2015), soft X-ray (Komossa & Bade 1999; Donley et al. 2002; Esquej et al. 2008; Maksym et al. 2010; Saxton et al. 2012, 2017; Bade et al. 2016), UV (Stern et al. 2004; Gezari et al. 2006, 2008, 2009) and optical (van Velzen et al. 2011; Gezari et al. 2012; Arcavi et al. 2014; Chornock et al. 2014; Holoien et al. 2014; Vinko et al. 2015) wavelengths. Some of the observed TDEs exhibit unusual properties. In particular, one of the detected TDEs shows an excess of variability in its light curve (Saxton et al. 2012) which can be explained if the black hole is actually a binary with a mass of $10^6\,M_\odot$, mass ratio of 0.1 and semimajor axis of 0.6 milliparsecs (Liu, Li & Komossa 2014). This candidate appears to have one of the most compact orbits among the known SMBH binaries and has overcome the 'final parsec problem' (Colpi 2014). Upon coalescence, it will be a strong source of gravitational wave emission in the sensitivity range of the evolved Laser Interferometer Space Antenna (eLISA). Three other TDEs appear to be very bright in X-rays with peak soft X-ray isotropic luminosity being highly super-Eddington (Burrows et al. 2011; Cenko et al. 2012; Brown et al. 2015), while follow-up observations showed that these events were also associated with bright, compact, variable radio synchrotron emission (Zauderer et al. 2011; Cenko et al. 2012). The observed high X-ray luminosity can be explained if the tidal disruption of stars in these cases powered a highly beamed relativistic jet pointed at the observer (Tchekhovskoy et al. 2014). Based on these three observations, Kawamuro et al. (2016) concluded that 0.0007 per cent–34 per cent of all TDEs source relativistic jets, while Bower et al. (2013) and van Velzen et al. (2013) estimated that $\lesssim$10 per cent of TDEs produce jetted emission at the observed level. Formation of jets in TDEs is a topic of active research, e.g. works by Metzger, Giannios & Mimica (2012), Mimica et al. (2015) and Generozov et al. (2017).

Based on the observations, the TDE rate was derived to be 10^{-4}–10^{-5} per year per galaxy (Donley et al. 2002; Esquej et al. 2008; Gezari et al. 2008; Luo et al. 2008; Maksym et al. 2010; Wang et al. 2012; Khabibullin & Sazonov 2014; van Velzen & Farrar 2014) and is consistent with order of magnitude theoretical predictions when IMBHs are ignored. The TDE rates were shown to be sensitive to the density profile and relaxation processes taking place in galactic nuclei (Magorrian & Tremaine 1999; Wang & Merritt 2004; Stone & Metzger 2016). The simplest and most commonly used estimate of the TDE rates is based on the steady-state solution of the Fokker–Planck equation describing the diffusion of stars in angular momentum and energy space driven by two-body relaxation. This process re-populates stellar orbits along which stars are disrupted by MBH, the so-called 'loss cone'. With the two-body relaxation being the main process to refill the loss cone, other processes that may contribute to the stellar budget were also discussed in the literature (Rauch & Tremaine 1996; Magorrian & Tremaine 1999; Merritt & Poon 2004; Ivanov, Polnarev & Saha 2005; Merritt & Wang 2005; Hopman & Alexander 2006; Perets et al. 2006; Chen et al. 2009, 2011; Wegg & Bode 2011; Liu & Chen 2013; Vasiliev & Merritt 2013; Vasiliev 2014; Merritt 2015; Lezhnin & Vasiliev 2015, 2016; Bar-Or & Alexander 2016; Li et al. 2017).

It is still unclear why IMBHs do not contribute to the observed TDEs, and most of the related theoretical studies show that black holes with masses smaller than $10^6\,M_\odot$ can disrupt stars at rates higher than those of higher masses (Wang & Merritt 2004; Stone & Metzger 2016). Therefore, if small haloes are occupied by IMBHs, most disruptions are expected to occur in these systems making TDEs particularly good probes of the poorly understood, low-mass end of MBH mass function (Stone & Metzger 2016). Moreover, once detected in large quantities, TDEs will offer insight into physics of quiescent black holes, probe extreme accretion physics near the last stable orbit, provide the means to measure the spin of black holes and probe general relativity in the strong-field limit (Guillochon et al. 2016; Hayasaki, Stone & Loeb 2016). In addition, jetted TDEs will allow us to explore processes through which relativistic jets are born.

In this paper, we extrapolate the population of TDEs to high redshifts (out to $z=20$), and predict their detectability with the next-generation X-ray telescopes (XRTs). We propose a new way to test the occupation fraction of IMBHs through their unique contribution to the X-ray luminosity function. The paper is organized as follows. We summarize our approach in Section 2, deriving TDE rates and outlining the TDE luminosity prescriptions. We show the intrinsic X-ray luminosity function in Section 3. Next, we make predictions for realistic next-generation X-ray surveys in Section 4 focusing on upgrades of *Swift* and *Chandra*. We summarize our conclusions in Section 5.

2 MODEL COMPONENTS

Even though TDEs have been extensively studied, the predicted rates are not in good agreement with observations. Therefore, we

adopt simple assumptions for the event rates from the literature with the aim to establish general trends in the redshift evolution of the TDE number counts and their observable signals. After defining the population of galaxies and black holes in Section 2.1, we start by considering rates in a given galaxy of halo mass $M_{\rm h}$ (Section 2.2) and generalize for a cosmological population of galaxies in Section 2.3. We discuss the luminosity of TDE flares in Section 2.4.

2.1 Galaxies and black holes

One of the key model ingredients that determines the TDE rates is the distribution of stars in galactic nuclei (Magorrian & Tremaine 1999; Wang & Merritt 2004). Depending on the merger history of the galaxy and the efficiency of feedback on star formation, the stellar density profile can develop either a core or a cusp. For simplicity, we adopt a singular isothermal sphere density profile $\rho(r) = \sigma^2/2\pi G R^2$ with σ being the constant velocity dispersion and R the halo virial radius. For a galaxy of halo mass $M_{\rm h}$, the relation between the halo mass and the velocity dispersion is simply $M_{\rm h} = 2\sigma^2 R/G$; while the velocity dispersion can be directly related to the black hole mass using the $M_{\rm BH}$–σ relation (Kormendy & Ho 2013; McConnell & Ma 2013; Baldassare et al. 2015; Saglia et al. 2016; Thomas et al. 2016)

$$M_{\rm BH} = 0.309 \times 10^9 \times \left(\sigma/200\ {\rm km\,s^{-1}}\right)^{4.38}\ {\rm M_\odot}, \quad (1)$$

which holds for a wide range of black hole masses from 5×10^4 $\rm M_\odot$ (Baldassare et al. 2015) to 1.7×10^{10} $\rm M_\odot$ (Thomas et al. 2016) in galaxies with a bulge (Guillochon & Loeb 2015). Assuming the isothermal stellar distribution, Wang & Merritt (2004) derived TDE rates for galaxies with a single central black hole, while Chen et al. (2009) report the rates in a case of a black hole binary. As we discuss in Section 2.2, for MBH with masses in the range $M_{\rm BH} \sim 10^5$–10^8 $\rm M_\odot$, the TDE rates per halo computed using the isothermal stellar distribution are similar (within tens of percent) to more realistic estimates based on a large galaxy sample (Stone & Metzger 2016), which justifies our assumption. The error in the rate estimation due to the idealized stellar density profile is small compared to other uncertainties, e.g. introduced by the poorly constrained occupation fraction of IMBHs in low-mass galaxies, which amounts to one–two orders of magnitude uncertainty in the derived volumetric TDE rates.

In order to address the uncertainty in the occupation fraction, $f_{\rm occ}$, of MBH, we consider two extreme cases: (i) complete black hole occupation of all haloes that form stars and (ii) assume that there are no black holes with masses below 10^6 $\rm M_\odot$, which is equivalent to the vanishing occupation fraction in haloes below 10^{10}–10^{11} $\rm M_\odot$ (depending on redshift). We refer to the former case as MBHs (or $f_{\rm occ} = 1$) and latter case as SMBHs (or $f_{\rm occ} = 0$). The two cases can be considered as an upper (former case) and lower (latter case) limits for the occupation fraction yielding, respectively, upper and lower limits for the expected TDE rates.

Even though black hole seeds could exist in even smaller haloes in the hierarchical picture of structure formation, one also needs stars to fuel a TDE flare. The lowest mass of a halo in which stars can form at high redshifts before the end of hydrogen reionization at $z \sim 6$ is determined by the cooling condition, which involves either molecular or atomic hydrogen (Tegmark et al. 1997; Loeb & Furlanetto 2013; Barkana 2016). The lowest temperature coolant, molecular hydrogen, forms stars in dark matter haloes as tiny as $\sim 10^5$ $\rm M_\odot$. However, hydrogen molecules are easily destroyed by radiative feedback (Machacek, Bryan & Abel 2001) in which case star formation proceeds via atomic cooling in haloes of 10^7–10^8 $\rm M_\odot$. Here, we neglect the molecular cooling channel and assume that before reionization, galaxies can form in haloes down to a velocity dispersion of $\sim 12\ {\rm km\,s^{-1}}$, which host black holes of mass $10^{3.1}$ $\rm M_\odot$. After reionization is complete, the smallest star-forming haloes are sterilized by photoheating feedback that evaporates gas out of all haloes with velocity dispersion less than $\sim 25\ {\rm km\,s^{-1}}$. As a result, small galaxies stop producing many stars and the loss cone of stars around the central black hole is most likely not refilled efficiently enough to support the equilibrium TDE rates. Therefore, we assume in the post-reionization era that all black holes below $\sim 10^{4.5}$ $\rm M_\odot$ remain without fuel and do not source TDEs. In a realistic reionization scenario, the minimal halo mass that efficiently forms stars would gradually increase with redshift (Sobacchi & Mesinger 2013; Cohen, Fialkov & Barkana 2016). However, because the reionization history is poorly constrained at present, we adopt the simplest scenario of instantaneous reionization at $z_{\rm re} = 8$, consistent with latest constraints by the *Planck* satellite (Planck Collaboration XLVII 2016). The minimal black hole mass in our MBH scenario is thus

$$M_{\rm BH,min} = \begin{cases} 10^{3.1}\ {\rm M_\odot}, & z \geq 8 \\ 10^{4.5}\ {\rm M_\odot}, & z < 8. \end{cases}$$

In our second, conservative, scenario we assume that $M_{\rm BH,min} = 10^6\,{\rm M_\odot}$. Several effects can contribute to low TDE rates from IMBHs, justifying our SMBHs scenario; black holes could be kicked out of haloes as a result of merger; radiation from AGNs could have negative feedback on star formation (AGN feedback); in this case, the loss cone would not be replenished. Another possible feedback mechanism is the stellar feedback from supernova explosions that can expel gas from the halo making star formation less efficient (Wyithe & Loeb 2013).

An additional model ingredient that determines the TDE rate is the merger history of a halo that we incorporate in Section 2.3. As discussed in Section 2.2, the TDE rate in a recently merged galaxy is boosted by several orders of magnitude for $\sim 10^5$ yr compared to a galaxy with a quiet merger history, e.g. works by Ivanov et al. (2005) and Chen et al. (2009, 2011). The enhanced TDE rates are explained by the fact that the dynamics of the system are changed by the presence of a black hole binary produced as a result of a merger.

2.2 TDE rates per halo

In the case of a single black hole, the most secure way to feed stars into the loss cone around the black hole is via the standard two-body relaxation, which sets a lower limit on the TDE rates between 10^{-4} and $10^{-6}\,{\rm yr^{-1}}$ (Frank & Rees 1976; Lightman & Shapiro 1977; Cohn & Kulsrud 1978; Magorrian & Tremaine 1999; Wang & Merritt 2004; Stone & Metzger 2016). Other processes that may contribute to the stellar budget include resonant relaxation (Rauch & Tremaine 1996; Hopman & Alexander 2006; Merritt 2015; Bar-Or & Alexander 2016), presence of massive perturbers such as stellar clusters or gas clouds (Perets et al. 2006), non-spherical geometry (Magorrian & Tremaine 1999; Merritt & Poon 2004; Vasiliev & Merritt 2013; Vasiliev 2014), black hole binaries (Ivanov et al. 2005; Chen et al. 2009, 2011; Wegg & Bode 2011; Liu & Chen 2013; Li et al. 2017) and anisotropy in the initial conditions (Merritt & Wang 2005; Lezhnin & Vasiliev 2015, 2016).

Assuming that the loss cone is refilled via two-body relaxation, the rate of tidal disruptions per halo per year for an isothermal stellar

distribution (Wang & Merritt 2004) reads

$$\dot{N}_{\rm TDE}^{1h} \sim 2.47\times10^{-4}\left(\frac{\sigma}{100\,{\rm km\,s^{-1}}}\right)^{7/2}\left(\frac{M_{\rm BH}}{10^7\,{\rm M_\odot}}\right)^{-1}\ {\rm yr^{-1}}, \quad (2)$$

where we only considered the disruption of solar mass stars[1]. Despite the fact that the stellar density used to derive equation (2) is idealized, the rates are similar to those derived by Stone & Metzger (2016) for stellar profiles from a real galaxy sample. Stone & Metzger (2016) estimated TDE rates due to two-body relaxation from ∼200 galaxies with $M_{\rm BH} \sim 10^5$–$10^{10}\,{\rm M_\odot}$ at $z \sim 0$ and got $\dot{N}_{\rm TDE} \sim 1.2\times10^{-5}\left(M_{\rm BH}/10^8{\rm M_\odot}\right)^{-0.247}$ for galaxies with a core and $\dot{N}_{\rm TDE} \sim 6.5\times10^{-5}\left(M_{\rm BH}/10^8\,{\rm M_\odot}\right)^{-0.223}$ for galaxies with a cusp. We checked that for our choice of $M_{\rm BH}$–σ relation, equation (2) gives similar rates in normalization (up to several tens of percents) and comparable slope of ~ -0.2 when compared to the cusp fit of Stone & Metzger (2016).

Although prominent TDEs from IMBHs are expected from the disruption of white dwarf stars (e.g. MacLeod et al. 2014) rather than solar mass stars, in this paper we consider disruption of solar mass stars only. This choice is well motivated because white dwarfs are formed at the end of the lives of main-sequence stars with masses below a few $\rm M_\odot$. Since such stars live for over a giga year, we do not expect many white dwarfs existing at high redshifts when the Universe was young. In addition, the very high redshift Universe was mostly populated by massive stars with masses between a few $\rm M_\odot$ and a few hundreds $\rm M_\odot$. Such stars end their lives as neutron stars, pair-instability supernovae, or black holes, never forming a white dwarf (Hirano et al. 2015). Our additional motivation is simplicity; given the great uncertainty in modelling the high-z TDEs, we prefer to simplify the model by fixing masses of the disrupted objects.

Modelling TDE rates in the merging system is more challenging, and rates are less understood than disruptions by a single MBH. Even though all theoretical studies point in the direction of TDE rates boosted for $\sim10^5$ yr by ∼2 orders of magnitude compared to the disruption by a single MBH, there is no consensus on details and it is unclear at present what is the leading process that replenishes the loss cone. When two galaxies merge, the black holes in the galactic cores first inspiral towards each other due to the dynamical friction. Next, when the mass in gas and stars enclosed within the black hole orbit is smaller than the total mass of the two black holes, the black holes become gravitationally bound and evolve as a binary. For black hole masses of $\sim10^6\,{\rm M_\odot}$, this occurs when the typical separation between the two black holes is ∼parsec. Gradually, the binary hardens. If the binary reaches separations $\lesssim$0.001 pc, gravitational waves are emitted as the two MBHs coalesce. Each one of the stages in the evolution of the binary has its own rate of TDEs. Using N-body simulations to model dry major mergers, Li et al. (2017) conclude that in the first stage, the tidal disruption rate for two well separated MBHs in the merging system has similar levels to the sum of the rates of two individual MBHs in two isolated galaxies. In their fiducial model, Li et al. (2017) find that after two MBHs get close enough to form a bound binary, the disruption rate is enhanced by a factor of 80 within a short time lasting for 13 Myr. This boosted disruption stage finishes after the SMBH binary evolves to a compact binary system, corresponding to a drop back of the disruption rate to a level few times higher than for an individual MBH. Other studies also point in the direction of enhanced rates from binaries. In particular, Ivanov et al. (2005) considered secular evolution of stellar orbits in the gravitational potential of an unequal mass binary and derived rates of 10^{-2}–1 TDEs per year per galaxy for a 10^6–10^7 $\rm M_\odot$ primary black hole and a binary mass ratio $q > 0.01$. The duration of this boosted disruption stage was determined by the dynamical friction time-scale

$$T_{\rm dyn} \sim \frac{2\times10^2(1+q)}{q}\left(\frac{10^7\,{\rm M_\odot}}{\rm M_{BH}}\right)^{1/2}{\rm yr}. \quad (3)$$

Chen et al. (2009) used scattering experiments to show that gravitational slingshot interactions between hardened binaries and a bound spherical isothermal stellar cusp will be accompanied by a burst of TDEs. It appears that a significant fraction of stars initially bound to the primary black hole will be scattered into the loss cone by resonant interaction with the secondary black hole. Chen et al. (2009) provide a fitting formula for the maximal TDE rates per halo with a binary MBH system

$$\dot{N}_{\rm TDE}^{2h} \sim (1+q)^{1/2}\left(\frac{\sigma}{100\,{\rm km\,s^{-1}}}\right)^4\left(\frac{M_{\rm BH}}{10^7\,{\rm M_\odot}}\right)^{-1/3}{\rm yr^{-1}} \quad (4)$$

and show that the enhancement lasts for $\sim10^4$ yr. Chen et al. (2011) included the Kozai–Lidov effect, chaotic three-body orbits, the evolution of the binary and the non-Keplerian stellar potentials and found that for masses of 10^7 and 10^5 $\rm M_\odot$, TDE rates 0.2 events per year last for $\sim3\times10^5$ yr that is three orders of magnitude larger than for a single black hole and broadly agrees with the conclusions of Chen et al. (2009). Wegg & Bode (2011) included the same processes as Chen et al. (2011) and arrived at similar rates. They found that the majority of TDEs are due to chaotic orbits in agreement with Chen et al. (2009), showing that the Kozai–Lidov effect plays a secondary role. Their rates are somewhat smaller than in Chen et al. (2009) largely because the authors consider less cuspy stellar profiles. Li et al. (2015) considered the evolution of stellar disruption around a binary with MBHs masses of 10^7 and 10^8 $\rm M_\odot$ due to the eccentric Kozai–Lidov mechanism yielding rate of 10^{-2} TDE per year for 5×10^5 yr. Finally, Liu & Chen (2013) concluded that the TDE rates of stars by SMBHs in the early phase of galaxy merger when galactic dynamical friction dominates could also be enhanced by several orders of magnitude (up to 10^{-2} events per year per galaxy) as a result of the perturbation by companion galactic core and the triaxial gravitational potential of the galactic nucleus.

To accommodate tidal disruptions induced by binary MBHs, we adopt the fitting function given by equation (4) assuming that this enhanced rate last for a dynamical time $T_{\rm dyn}$, while for the rest of the time the TDE rate is simply $\dot{N}_{\rm TDE}^{1h}$. As we can derive from equations (2) and (4), the scaling of TDE rates with $M_{\rm BH}$ is different for single and binary MBHs. Applying the $M_{\rm BH}$–σ relation to equations (2) and (4), we find that the TDE rate scales as $\dot{N}_{\rm TDE}^{2h} \propto M_{\rm BH}^{0.6}$ for binaries and $\dot{N}_{\rm TDE}^{1h} \propto M_{\rm BH}^{-0.2}$ for single black holes. This property has immediate implications to the total observable TDE rates that will be discussed in Section 4.

2.3 Number of TDEs across cosmic time

The observed TDE number counts per unit time that originate from redshift z depends on several factors with the dominant factor being the amount of haloes of each mass and their merger history. To determine the halo abundance, we make use of the Sheth–Tormen mass function (Sheth & Tormen 1999) in calculating the comoving number density of haloes in each mass bin $\rm d$$N_{\rm h}$/$\rm d$$M_{\rm h}$ in units of

[1] The dependence of equation (2) on stellar mass can be re-introduced by adding a factor $(m_*/{\rm M_\odot})^{-1/3}(r_*/{\rm R_\odot})^{1/4}$ with $r_* = {\rm R_\odot}\,(m_*/{\rm M_\odot})^{0.8}$ for stars along the lower main sequence.

$M_\odot^{-1}\,\mathrm{Mpc}^{-3}$. Next, adopting the merger rates of Fakhouri, Ma-P. & Boylan-Kolchin (2010), we calculate the dimensionless average merger rate $\mathrm{d}N_\mathrm{m}/\mathrm{d}\zeta\,/\mathrm{d}z$ (in units of mergers per halo per unit redshift per unit halo mass ratio, ζ), given by a fitting formula

$$\frac{\mathrm{d}N_\mathrm{m}}{\mathrm{d}\zeta\,\mathrm{d}z}(\mathrm{M},\zeta,z)=A\left(\frac{\mathrm{M}}{10^{12}\,\mathrm{M}_\odot}\right)^{\alpha}\zeta^{\beta}\exp\left[\left(\frac{\zeta}{\bar{\zeta}}\right)^{\gamma}\right](1+z)^{\eta}, \quad (5)$$

where $(\alpha,\beta,\gamma,\eta)=(0.133,-1.995,0.263,0.0993)$ and $(A,\bar{\zeta})=(0.0104,9.72\times10^{-3})$.

For each halo, we assign a TDE rate of $\dot{N}^{2h}_\mathrm{TDE}$ according to the probability, P_2, of it to encounter a recent merger, and $\dot{N}^{1h}_\mathrm{TDE}$ with a probability $P_1=1-P_2$. The probability, P_2, is determined using the following criterion: if the time between mergers is larger than the dynamical time, the TDE rates are those of single MBH, while if the time between mergers is smaller than T_dyn, there is an enhancement due to binaries. Given the merger rates, we estimate the probability of a halo of mass M_h at redshift z to be a result of a recent merger as follows:

$$P_2(M_\mathrm{h},z)=1-\exp\left[-T_\mathrm{dyn}\lambda\right],$$

where

$$\lambda=\int\mathrm{d}\zeta\,\frac{\mathrm{d}N_\mathrm{m}}{\mathrm{d}z\mathrm{d}\zeta}\frac{\mathrm{d}z}{\mathrm{d}t}. \quad (6)$$

For very light haloes, mergers are frequent and haloes typically undergo several mergers within T_dyn, in which case the probability for a merger is near unity. We assume that probability for merger with black hole mass ratio q is flat for $q=10^{-3}$ to 10^{-1}, and q is related to the halo mass ratio, ζ, through equation (1). We ignore mergers with $0.1<q<1$ as they are expected to be rare. The top panel of Fig. 1 shows the halo mass weighted number density of mergers $\int\mathrm{d}M_\mathrm{h}P_2\mathrm{d}N_\mathrm{h}/\mathrm{d}M_\mathrm{h}$ that yield enhanced TDE rates per unit volume in cases of $f_\mathrm{occ}=0$ (SMBHs only) and $f_\mathrm{occ}=1$ (all MBHs). In each case, the integral is over haloes whose progenitors have both large enough black holes and gas to form stars. Such mergers are rare when the minimal mass is high (SMBH case), especially at high redshifts. In the case of $f_\mathrm{occ}=1$, we can clearly see the turn on of photoheating feedback at $z=8.8$ that shuts down star formation in galaxies below $M_\mathrm{h}\sim10^9\,\mathrm{M}_\odot$ at lower redshifts leading to suppressed TDE rates.

Having the proper probabilities, we can now calculate the expected TDE rates for an observer as a function of redshift. At every given redshift, P_1 haloes in each mass bin host a single MBH yielding the TDE rate

$$\dot{N}^1_\mathrm{TDE}=\int\mathrm{d}M_\mathrm{h}\frac{\mathrm{d}N_h}{\mathrm{d}M_\mathrm{h}}P_1\frac{\dot{N}^{1h}_\mathrm{TDE}}{(1+z)}. \quad (7)$$

The factor $(1+z)$ compensates for the time dilation in the apparent rate. The contribution from binaries is given by

$$\dot{N}^2_\mathrm{TDE}=\int\mathrm{d}M_\mathrm{h}\frac{\mathrm{d}N_h}{\mathrm{d}M}\int\mathrm{d}q\frac{\mathrm{d}P_2}{\mathrm{d}q}\frac{\dot{N}^{2h}_\mathrm{TDE}}{(1+z)}. \quad (8)$$

The expected TDE rates per year per unit comoving volume from single and binary MBHs, $\dot{N}^1_\mathrm{TDE}$ and $\dot{N}^2_\mathrm{TDE}$, are shown in the bottom panel of Fig. 1.

As was pointed out above, TDE rates induced by binary black holes are higher in the high black hole mass end, while the single black hole systems are more efficient in the low black hole mass end. To demonstrate this feature, we show in Fig. 2 the fraction of intrinsic events [with no $(1+z)$ factor] sourced by single black holes out of total number of TDEs at $z=0$ and 5 as a function of the black hole mass (total mass in the case of binaries) in solar mass

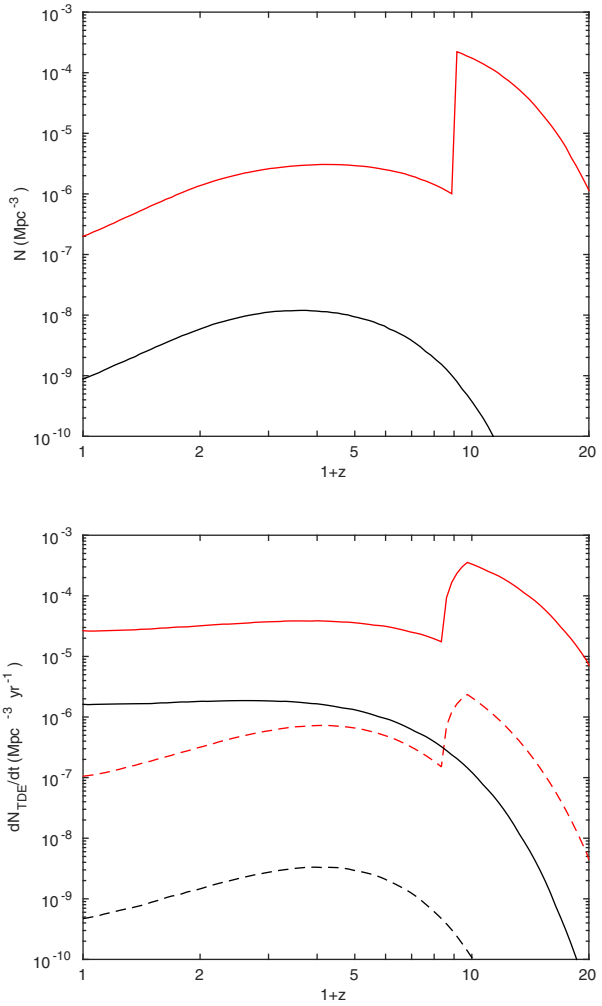

Figure 1. Top: halo mass averaged number density of systems with mergers that occurred at $t<T_\mathrm{dyn}$. We show the case of SMBHs only ($f_\mathrm{occ}=0$, black) and all MBHs ($f_\mathrm{occ}=1$, red). Bottom: intrinsic TDE rates in the observer's frame per comoving volume as a function of redshift are shown for SMBHs only (black) and all MBHs (red). In each case, we show the contribution of single black holes with rates from Wang & Merritt (2004, solid, $\dot{N}^{1h}_{TDE}$) and contribution of binaries (dashed, $\dot{N}^{2h}_\mathrm{TDE}$) assuming solar mass stars. In all cases with mergers, we assume that the enhancement due to binaries lasts for T_dyn.

units for $f_\mathrm{occ}=0$ and 1. As expected from the TDE scaling with the black hole mass ($\propto M^{0.6}_\mathrm{BH}$ for binaries and $\propto M^{-0.2}_\mathrm{BH}$ for single black holes), binary systems dominate at large black hole masses and at high redshifts (because of the increased merger rates). The mass dependence determines contribution of each component to the overall luminosity function of the TDEs which we consider in the next section.

Finally, in our cosmological model we assume that 10 per cent of all TDEs source relativistic jets with the Lorenz factor of the order of $\Gamma=10$ based on X-ray observations of jetted TDE (Burrows et al. 2011). In the spirit of our simple approach, we ignore parameters such as stellar magnetic fields (Guillochon & McCourt 2017), which could affect fraction of jetted TDEs and assume a constant jet fraction over the halo mass and redshift range. Because the luminosity is channelled into a collimated beam of an opening angle $\theta\sim1/\Gamma$, only a small fraction of the jetted TDEs will be actually observable. For an observer, the

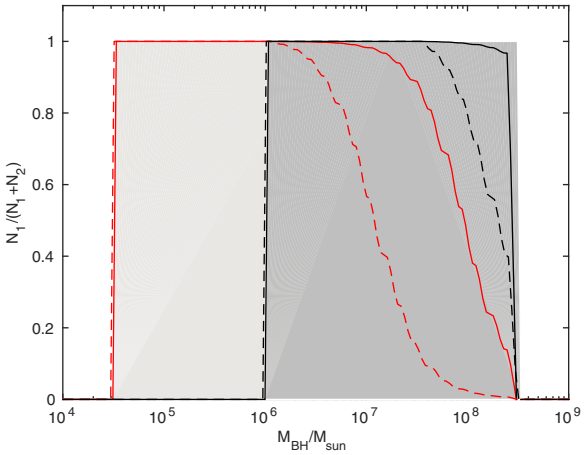

Figure 2. Fraction of intrinsic disruption events sourced by single black holes versus black hole mass for SMBHs only ($f_{\rm occ} = 0$, black curves) and all MBHs ($f_{\rm occ} = 1$, red curves). We show the fraction at $z = 0$ (solid) and $z = 5$ (dashed). The dark grey region marks the occupation of SMBH, whereas the pale grey refers to the occupation of IMBHs.

fraction of sky covered by the jets pointing towards the observer is, thus, $f_{\rm jet} = 10$ per cent $\times\, 2 \times \pi\theta^2/4\pi = 5 \times 10^{-2}$ per cent where we accounted for two jets emitted by every system. Overall, the observed TDE rates will include 90 per cent of non-jetted TDE and $f_{\rm jet}$ of TDE with jets where we account only for the events that point towards the observer.

2.4 Luminosity of TDE flares

The TDE rates shown in Fig. 1 are not the ones we would actually observe. Observable rates depend on the luminosity (observed flux) of each event as well as on the sensitivity of a telescope (discussed in the next section). In this section, we outline our assumptions for the TDE luminosity and use them in Section 4 to calculate the observable signals. Because we are mainly interested in the high-redshift events that could be observed in X-rays when relativistic jets are produced, we will focus on the TDE signature in X-rays ignoring their UV and optical counterparts. We are also largely ignoring radio signals because it is unclear whether or not the radio emission from the TDE sourced jets arises from the same regions as their X-ray emission.

The three X-ray observations of TDEs with jets include: (1) SwiftJ164449.3+573451, hereafter Sw1644+57 (Bloom et al. 2011; Burrows et al. 2011; Levan, Tanvir & Cenko 2011), of peak X-ray isotropic luminosity $L_{\rm X} \sim 4 \times 10^{48}\,{\rm erg\,s^{-1}}$ that originated from a galaxy at $z = 0.353$ and was discovered in 2011 March by the *Swift* Burst Alert Telescope (BAT, 15–150 keV; Barthelmy et al. 2005); (2) SwiftJ2058.4+0516, hereafter SwJ2058+05 (Cenko et al. 2012), of peak X-ray isotropic luminosity equivalent to $L_{\rm X} \sim 4 \times 10^{48}\,{\rm erg\,s^{-1}}$, which was discovered at $z = 1.185$ in 2011 May by the BAT as part of the hard X-ray transient search and (3) SwiftJ1112.2−8238, hereafter Sw1112-82 (Brown et al. 2015), which was detected by BAT in 2011 June as an unknown, long-lived γ-ray transient source in a host identified at $z = 0.89$ and with $L_{\rm X} \sim 6 \times 10^{48}\,{\rm erg\,s^{-1}}$. Estimates of the SMBH mass in each one of these events yield $M_{\rm BH} \sim 10^6$–$10^7\,{\rm M_\odot}$. Because the Eddington luminosity for a black hole of mass $M_{\rm BH}$ is only $L_{\rm Edd} = 1.3 \times 10^{38}(M_{\rm BH}/{\rm M_\odot})\,{\rm erg\,s^{-1}}$, these events either are intrinsically highly super-Eddington or the emitted energy is channelled in tightly collimated jets and the luminosity is boosted by a factor of $\sim 10^3$–10^4.

Theory predicts that a flare is produced when debris return to the vicinity of a black hole $t_{\rm fall} \approx 0.1(M_{\rm BH}/10^6\,{\rm M_\odot})^{1/2}$ yr after the disruption and forms an accretion disc. If a solar mass star is completely disrupted, its debris fallback rate is (Rees 1988; Phinney 1989; Stone et al. 2013)

$$\dot{M}_{\rm fall} \sim \frac{1}{3t_{\rm fall}} \left(\frac{t}{t_{\rm fall}}\right)^{-5/3} {\rm M_\odot\ yr^{-1}} \tag{9}$$

with the peak mass accretion rate value of

$$\frac{\dot{M}_{\rm peak}}{\dot{M}_{\rm Edd}} = 133 \left(\frac{M}{10^6\,{\rm M_\odot}}\right)^{-3/2}, \tag{10}$$

where the Eddington accretion rate is $\dot{M}_{\rm Edd} = L_{\rm Edd}/\eta c^2$ and $\eta \sim 0.1$ is a typical radiative efficiency. It is likely that the mass fallback rate can be directly related to the observed X-ray luminosity of the source and, thus, can be used to determine the total emitted energy. In particular, if the accretion rate is fully translated to the bolometric luminosity, the peak luminosity is $L_{\rm peak} = \eta c^2 \dot{M}_{\rm peak}$. However, it is still not clear what is the efficiency of this process especially for intermediate black holes with mass less than 50 million solar masses for which $L_{\rm peak}$ is highly super-Eddington for efficient circularization of the debris (Dai, McKinney & Miller 2015; Shiokawa et al. 2015; Guillochon et al. 2016).

Super-Eddington accretion fuelled by a tidal disruption of a star was both studied in numerical simulations (Jiang, Stone & Davis 2014; McKinney et al. 2014; Sądowski et al. 2015; Sądowski & Narayan 2015; Inayoshi, Haiman & Ostriker 2016; Sakurai, Inayoshi & Haiman 2016) and detected in nature (in the jetted TDE event Sw1644+57) based on observations of reverberation in the redshifted iron Kα line (Kara et al. 2016). From the reverberation time-scale, the authors estimate the mass of the black hole to be a few million solar masses, suggesting an accretion rate of at least 100 times the Eddington limit. In simulations, super-Eddington luminosities are inferred: Jiang et al. (2014) studied super-Eddington accretion flows on to black holes using a global three-dimensional radiation magnetohydrodynamical simulation and found mass accretion rate of $\dot{M} \sim 220\,L_{\rm Edd}/c^2$ with outflows along the rotation axis, and radiative luminosity of $10\,L_{\rm Edd}$; $\dot{M} \sim 400\,L_{\rm Edd}/c^2$ was measured for a $10\,{\rm M_\odot}$ black hole with peak luminosity of $50\,L_{\rm Edd}$ (McKinney, Dai & Avara 2015); Inayoshi et al. (2016) argued that $\dot{M} \sim 5000\,L_{\rm Edd}/c^2$ is limited to the Eddington luminosity in a metal-poor environment, but Sakurai et al. (2016) find $1 < L/L_{\rm Edd} < 100$. In other simulated systems, non-relativistic beaming was shown to boost the apparent (observed) luminosity (e.g. Sądowski et al. 2015). Although the overall radiative efficiency and luminosity of these jets are still debated, in simulations a strong outflow is generated and radiation can leak through a narrow funnel along the polar direction. Close to the black hole, a jet carves out the inner accretion flow, exposing the X-ray emitting region of the disc. Sądowski et al. (2015) found that if a source with a moderate accretion rate is observed down the funnel, the apparent luminosity of such a source will be orders of magnitude higher than the non-jetted luminosity. Sądowski & Narayan (2015) showed that for an observer viewing down the axis, the isotropic equivalent luminosity is as high as $10^{48}\,{\rm erg\,s^{-1}}$ for a $10^7\,{\rm M_\odot}$ black hole accreting at 10^3 the Eddington rate, which agrees with the observations of jetted TDEs. Independent of the accretion rate in simulations, super-Eddington discs around black holes exhibit a surprisingly large efficiency of $\eta \sim 4$ per cent for non-rotating black holes; while spinning black holes yield the maximal efficiency of jets of 130 per cent (Piran, Sądowski & Tchekhovskoy 2015).

Overall, it is still not clear whether there is a connection between relativistic beaming and super-Eddington accretion. On one hand, Kara et al. (2016) argued that Sw1644+57 was not a relativistic event, because reverberation is never detected in blazars with highly relativistic jets. On the other hand, simulations suggest that relativistic beaming can explain observed super-Eddington luminosities indicating that once the accretion is super-Eddington, relativistic jets can be produced (McKinney et al. 2014). In addition, Burrows et al. (2011) argued that Sw1644+57 has indeed powered a relativistic jet.

Because the TDE flares in jetted events are not fully understood, we aim to provide plausible limits for the observed luminosity function of high-redshift TDE events. We (i) assume that 10 per cent of the events trigger relativistic jets with the Lorentz factor $\Gamma = 10$, as mentioned at the end of Section 2.3 and (ii) use two simple approaches to determine first the bolometric and then the X-ray luminosity of each TDE. Our first approach (Model A) is to simply assign the Eddington luminosity to each event according to the black hole mass, $L^{\rm A}_{\rm TDE} = L_{\rm Edd}$. The second approach (Model B) assumes that the TDE bolometric luminosity is proportional to the mass accretion rate. However, for IMBHs the peak accretion rate exceeds both the observed rates and the simulated ones by few orders of magnitude. As studies have shown, TDE luminosity is not likely to exceed few hundreds $L_{\rm Edd}$ (Jiang et al. 2014; McKinney et al. 2014; Sądowski et al. 2015; Sądowski & Narayan 2015; Inayoshi et al. 2016; Sakurai et al. 2016). Therefore, we adopt an upper limit of $300\,L_{\rm Edd}$ and the luminosity of each event reads

$$L^{\rm B}_{\rm TDE} = \min\left[L_{\rm peak}, 300\,L_{\rm Edd}\right]. \quad (11)$$

The major distinction between Models A and B is that in Model A the brightest events are produced by the biggest black holes that also are the rarest ones, especially at high redshifts; while when the luminosity scales as the accretion rate with a ceiling (Model B), the most luminous events are produced by black holes of mass $M_{\rm BH} \sim 2.5 \times 10^6\,{\rm M}_\odot$ that are more common.

Observations show that the X-ray luminosity of the three jetted TDEs has a spectral energy distribution (SED) well fitted by a power law $S_\nu \propto \nu^{-\alpha}$ with a spectral index α in the range of 0.3–1 with $\alpha = 0.33$ for Sw1112−82, $\alpha \sim 0.8$ for Sw1644+57 and $\alpha \sim 0.6$ for SwJ2058+05. Therefore, in our modelling we adopt power-law SED with a unique spectral index of $\alpha = 0.5$ to describe all the jetted events. The SED of a non-jetted TDE is expected to be a combination of a power law and a blackbody, where the latter is negligible at high enough energies (∼1 keV and above; Kawamuro et al. 2016). We follow Kawamuro et al. (2016) assuming that the spectral index, α, is the same for non-jetted events as for the jetted ones ($\alpha = 0.5$). The intrinsic spectral luminosity of an event is thus $L_\nu = L_0\nu^{-\alpha}$, where L_0 is the normalization constant. Assuming that the SED of these objects over a wide wavelength range is similar to that of AGNs, we can calculate the X-ray luminosity of each event based on its bolometric luminosity. For the soft X-ray band (2–10 keV), we adopt a bolometric correction factor of $k_{2-10} \sim 50$ for the Eddington and $k_{2-10} = 70$ for the super-Eddington accretion rates (Vasudevan & Fabian 2007; Kawamuro et al. 2016). Given these numbers, we normalize our power-law spectra in the soft X-ray band so that $L_0 = k_{2-10}\,(1-\alpha)\,L_{\rm TDE}[10^{1-\alpha} - 2^{1-\alpha}]^{-1}$. Using this prescription, we can calculate the observed spectral flux for non-jetted TDEs at redshift z

$$S_\nu = \frac{L_0\nu^{-\alpha}(1+z)^{1-\alpha}}{4\pi D_{\rm L}^2}, \quad (12)$$

where $D_{\rm L}$ is the luminosity distance to the source. The observed flux of a jetted event and observed frequency ν are boosted by the factor of $\mathcal{D}^{3+\alpha}$, where $\mathcal{D} = [\Gamma(1-\beta\cos\theta)]^{-1}$ is the Doppler factor (Burrows et al. 2011), and $\Gamma = 1/\sqrt{1-\beta^2}$ with $\beta = v/c$ the speed of the ejecta in units of the speed of light, c.

Simulations show that TDEs occurring around MBH binaries have similar peak luminosity in X-rays as TDEs sourced by single black holes; however, the light curve has stronger variability in time due to the perturbations introduced by the secondary black hole (Liu, Li & Chen 2009; Liu et al. 2014; Coughlin et al. 2016; Ricarte et al. 2016). Therefore, we adopt a similar prescription as described above to assigned X-ray luminosity to TDEs sourced by binaries.

3 INTRINSIC LUMINOSITY FUNCTION

We can now make predictions for the intrinsic X-ray luminosity function of TDEs in the two cases of SMBHs and MBHs. It appears that, because TDE rates from single and binary black holes scale differently with $M_{\rm BH}$, binaries contribute the brightest TDE flares for both Models A and B. However, this contribution is significant only when small dark matter haloes are occupied by IMBHs providing enough progenitors to form SMBH binaries. In case only SMBHs populate haloes, TDEs from binaries occur only in systems with both black holes of $M_{\rm BH} > 10^6\,{\rm M}_\odot$ which are extremely rare and contribute at most few per cent of the brightest TDE flares.

The fraction of events brighter than $10^{45}\,{\rm erg\,s^{-1}}$ (which is close to the Eddington luminosity of an $M_{\rm BH} = 10^7\,{\rm M}_\odot$ black hole) is shown on Fig. 3. To reinforce this point, we list in Table 1 the percentage of events brighter than $10^{45}\,{\rm erg\,s^{-1}}$ produced by binary black holes at redshifts $z = 0$, 0.5, 1, 2, 5, 7, 10 and 15. The role of binaries becomes more important at higher redshifts where mergers are more frequent. In the case of fully occupied haloes, binaries start dominating the bright events at $z = 1$ in Model A and their contribution increases with redshift; while in Model B the maximal fraction of bright TDEs sourced by binaries is only ∼11 per cent in the post-reionization era ($z \lesssim 8$). In both Models A & B with $f_{\rm occ} = 1$, we find a sudden increase in the binary contribution at $z > 8$ (pre-reionization era) when the photoheating feedback is not active. In the case of $f_{\rm occ} = 0$, as expected, the fraction of binaries is at most few per cent and varies smoothly with redshift as this population is not affected by the photoheating feedback. With next-generation XRT that could statistically analyse high-redshift TDEs, the change in TDE number counts with redshift could be a smoking gun of feedback processes or a marker of the black hole occupation fraction.

We conclude this section by showing the expected cumulative X-ray luminosity function in Fig. 4 versus X-ray luminosity in the observed 1–150 keV band. Our results are presented for both SMBHs and MBHs. In the case of MBHs, there are four distinct terms (shown separately on the figure) that affect the luminosity function, i.e. the contributions from single and binary black holes of jetted and non-jetted events. Each one of the four terms contributes a knee and dominates specific luminosity regime. On the other hand, our SMBH model has only two distinct features because in this case mergers have a negligible contribution and the knees in the luminosity function result from the jetted and non-jetted population of TDEs produced by single black holes. The shape of the luminosity function alone could be used to place limits on the occupancy of the IMBHs once a complete compilation of TDEs is available.

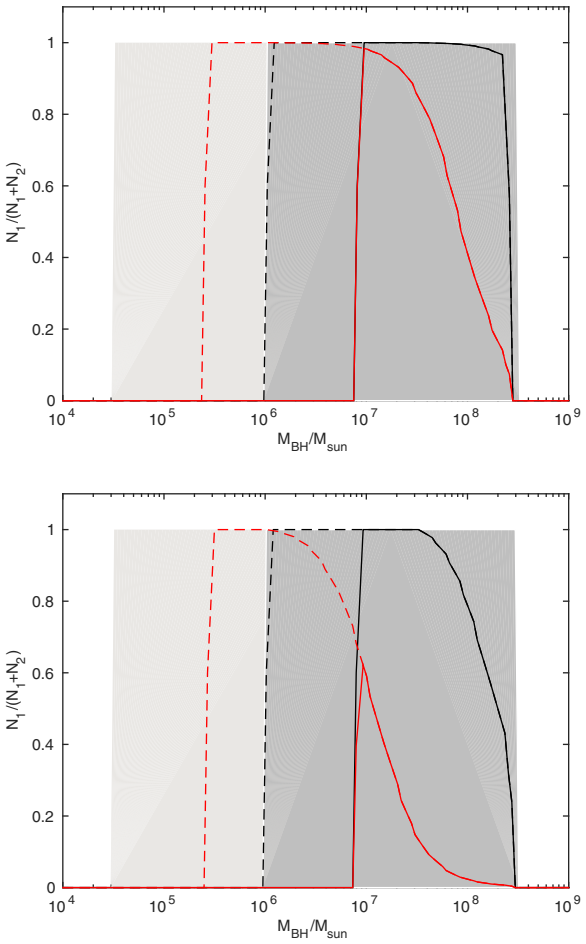

Figure 3. Fraction of TDEs brighter than an intrinsic luminosity $L > 10^{45}$ erg s^{-1} (close to the Eddington luminosity of $M_{\rm BH} = 10^7\,{\rm M}_\odot$) that are sourced by single MBHs, $N^1_{\rm TDE}/(N^1_{\rm TDE} + N^2_{\rm TDE})$, as a function of $M_{\rm BH}$ at $z = 0$ (top) add $z = 5$ (bottom). We show the case of Models A (solid) and B (dashed) for SMBHs (black) and MBHs (red). The dark grey region marks the occupation of SMBHs, with pale grey referring to IMBHs.

Table 1. Percentage of TDE produced by binary black holes: all events (third column), only bright events with intrinsic luminosity $L > 10^{45}$ erg s^{-1} for Model A (fourth column) and Model B (fifth column).

Model	Redshift	All	Bright (A)	Bright (B)
$f_{\rm occ} = 1$	$z = 0$	0.4 per cent	25.2 per cent	2.1 per cent
	$z = 0.5$	0.7 per cent	38.3 per cent	3.6 per cent
	$z = 1$	1.0 per cent	50.8 per cent	5.1 per cent
	$z = 2$	1.6 per cent	66.7 per cent	8.7 per cent
	$z = 5$	1.5 per cent	83.8 per cent	11.1 per cent
	$z = 7$	0.9 per cent	85.7 per cent	8.3 per cent
	$z = 8$	0.9 per cent	98.2 per cent	68.6 per cent
	$z = 10$	0.5 per cent	98.4 per cent	69.8 per cent
	$z = 15$	0.1 per cent	98.8 per cent	74.4 per cent
$f_{\rm occ} = 0$	$z = 0$	<0.1 per cent	0.2 per cent	<0.1 per cent
	$z = 0.5$	<0.1 per cent	0.3 per cent	<0.1 per cent
	$z = 1$	<0.1 per cent	0.5 per cent	<0.1 per cent
	$z = 2$	0.2 per cent	0.9 per cent	0.2 per cent
	$z = 5$	0.2 per cent	2.2 per cent	0.2 per cent
	$z = 7$	0.1 per cent	2.2 per cent	0.1 per cent
	$z = 8$	0.1 per cent	2.2 per cent	0.1 per cent
	$z = 10$	<0.1 per cent	1.8 per cent	<0.1 per cent
	$z = 15$	<0.1 per cent	0.5 per cent	<0.1 per cent

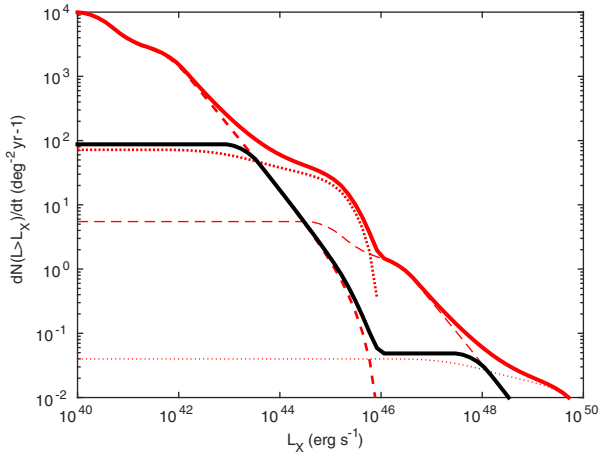

Figure 4. Number of events per year detected by an ideal instrument of a field of view of 1 deg^2 versus X-ray luminosity in the observed 1–150 keV band. We show the cumulative luminosity functions assuming sources with Eddington luminosity (Model A), with $f_{\rm occ} = 1$ (red, thick solid) and $f_{\rm occ} = 0$ (black, thick solid). In the $f_{\rm occ} = 1$ case, we also show contributions due to various components: non-jetted events sourced by single black holes (thick dashed red) and binary black holes (thin dashed red), jetted events sourced by single black holes (thick dotted red) and binary black holes (thin dotted red). The brightest events are dominated by jetted TDEs sourced by binary black holes, but these are very rare.

4 OBSERVATIONAL SIGNATURE

Number of disruption events that are actually detected by a telescope depend on its flux limit and field of view. Here, we will focus on telescopes such as *Swift* and *Chandra* and explore signals that next-generation X-ray missions could probe. Bright X-ray transients such as GRBs or jetted TDEs are detected when they first trigger the BAT on *Swift*. The trigger occurs if the signal's flux rises above 28.8×10^{-11} erg cm^{-2} s^{-1} in the hard X-ray band (15–150 keV), i.e. reaches the 6σ statistical significance of BAT (Barthelmy et al. 2005). Interestingly, all three jetted TDEs were detected by *Swift* over a period of three consecutive months, which suggests the possibility that further examples may be uncovered by detailed searches of the BAT archives. The XRT is another instrument on board *Swift* observing in the soft X-ray band (0.2–10 keV) and reaching 2×10^{-14} erg cm^{-2} s^{-1} sensitivity in 10^4 s with a 23.6×23.6 arcmin^2 field of view. (Because soft X-ray photons below ∼1 keV can be absorbed by dust, we will quote numbers in the observed 2–10 keV band when referring to soft X-rays.) As we show below, a telescope with such field of view and sensitivity as XRT is good for follow-up observations of TDEs; while either a larger field of view or sensitivity are required to detect TDEs in large quantities. In fact, a telescope such as *Chandra* with its high point source sensitivity of $\sim 4 \times 10^{-15}$ erg cm^{-2} s^{-1} in 10^4 s (or $\sim 4 \times 10^{-17}$ erg cm^{-2} s^{-1} in 10^6 s) over 0.4–6 keV band and field of view of $\sim 15 \times 15$ arcmin^2, could have many TDEs per frame, as we argue below.

Following Woods & Loeb (1998), the observed number of new events per year seen by BAT in the 15–150 keV band with peak flux larger than the flux limit $S_{\rm lim}$ is given by

$$\dot{N}^{S>S_{\rm lim}}_{\rm TDE} = \int_0^{z_{\rm max}} \int_{S_{15-150}>S_{\rm lim}} \frac{\dot{N}_{\rm TDE}}{(1+z)} \frac{{\rm d}V}{{\rm d}z} {\rm d}z {\rm d}S, \quad (13)$$

where S_{15-150} is the observed peak flux produced by each event. This equation is appropriate for threshold experiments, such as BAT, observing a population of transient sources that are standard candles

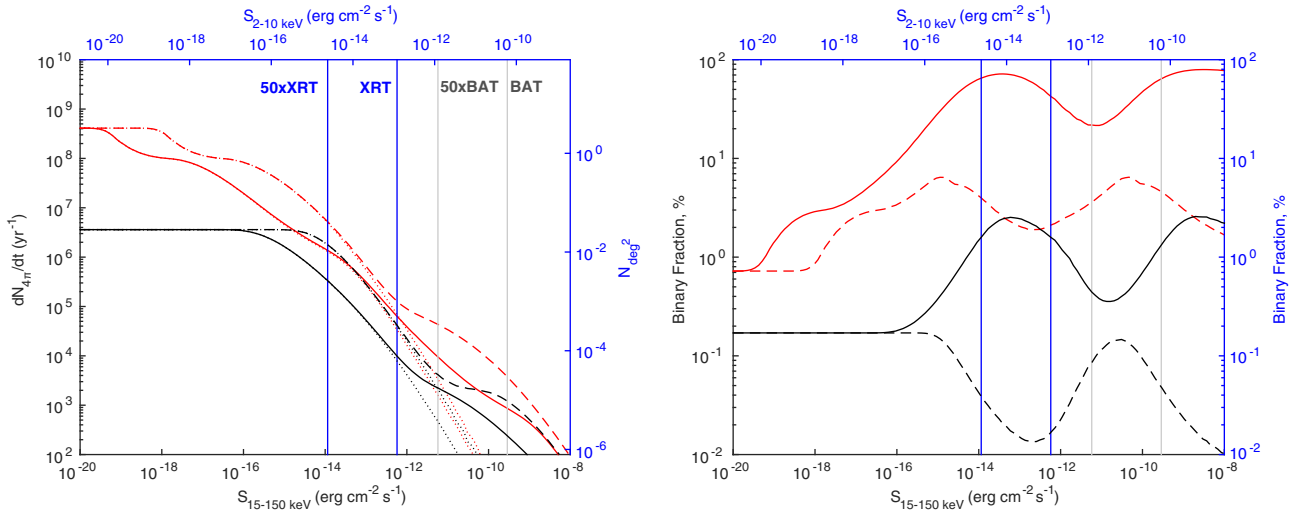

Figure 5. Left: cumulative all-sky number of TDEs brighter than the given flux limit $S_{15-150\,\mathrm{keV}}$. The bottom (black) axis labels refer to survey mode observations in the 15–150 keV band with the left vertical axis showing the TDE rates per sky per year. Grey vertical lines show 6σ BAT sensitivity of 2.88×10^{-10} erg cm^{-2} s^{-1} and a 50 times better sensitivity of a future instrument ('50 ×BAT'). The upper (blue) coordinate system corresponds to snapshot mode observations in the 2–10 keV band with the right vertical axis showing the number of TDE observed per snapshot of integration time $t_{\rm int} = 1 \times 10^4$ s in a field of view of 1 deg^2 and blue vertical lines showing 6σ XRT sensitivity of 1.2×10^{-13} erg cm^{-2} s^{-1} and a 50 times better sensitivity of an instrument ('50 ×XRT'). We show the results for SMBHs (black) and MBHs (red) for Models A (solid) and B (dashed). In all cases, we have accounted for the contribution of both single and binary black holes, as well as for 10 per cent jetted events that are visible out to higher redshifts. The non-jetted contribution is shown with dotted lines in each case. Right: fraction of TDEs (in percent) above the flux limit that are contributed by binary systems. We use the same colour code as in the left-hand panel.

in a peak flux. Fig. 5 shows the total rates of events with observed flux greater than $S_{\rm lim}$ produced at all redshifts including jetted and non-jetted TDEs produced by both single and binary black holes. The black coordinate system in the figure shows the total number of hard X-ray events observed per year over the entire sky (field of view of 4π) and for a 100 per cent duty cycle as a function of the telescope flux limit $S_{\rm lim}$, in the cases of our Models A and B and for $f_{\rm occ} = 0$ and 1.

As seen from Fig. 5 where the contribution of non-jetted TDEs is labelled by a dotted line for each scenario, the expected number counts are dominated by jetted TDEs at the BAT sensitivity limit since the non-jetted contribution is negligible. To compare our predictions to BAT observations, we need to re-scale the rates correcting for the limited field of view and duty cycle of the telescope. First, assuming that three jetted TDEs were detected by BAT in 9 yr of *Swift* lifetime with the duty cycle of 75 per cent over $4\pi/7$ of the sky we get $\dot{N}_{\rm TDE} = 3\,{\rm yr}^{-1}$, while making use of the fact that the events were detected in three consecutive months (i.e. BAT sees 1 TDE per month), we get 112 TDEs per year. The latter number can be interpreted as a reasonable lower limit on the occurrence rate of jets and is just a factor of ∼2 lower than our predictions for $f_{\rm occ} = 0$ (Model A) and a factor of ∼8 for $f_{\rm occ} = 1$. The discrepancy could be explained by both observational limitations and modelling uncertainties, e.g. the assumed jetted fraction of 10 per cent might be overestimated. For a next-generation survey with 50 times better sensitivity than BAT, i.e. going from the BAT configuration to '50 × BAT', our model predicts 11 times more sources for $f_{\rm occ} = 1$ and 3–9 more sources for $f_{\rm occ} = 0$ (see Table 2 for details).

In Table 3, we list the fraction of observable TDEs produced by binaries (in per cents) for each model and telescope sensitivity limit. At BAT sensitivity limit and in the case of high occupancy of IMBHs considerable fraction of observable TDEs are sourced by binary systems (∼60 per cent for Model A and ∼5 per cent for Model B). As expected, because most of the faint systems are contributed by single MBHs, the fraction decreases as the sensitivity of the telescope improves. However, the decrease is non-monotonic as a function of $S_{\rm lim}$ (as evident from the right-hand panel of Fig. 5), because of the contributions from different components (with/without jets, single and binary MBHs). In the case of a low occupancy, the contribution of binaries to the TDE sample is always below 2 per cent. The contribution of binaries, and thus

Table 2. For each model, we show the statistics of the observed events depending on the telescope sensitivity. TDE rates per sky per year (and divided by a factor of 10^3, $\dot{N}^{4\pi,A}_{\rm TDE}/10^3$) are shown for Model A for sources at all redshifts (third column) and at $0 < z < 3$ (fourth column); for Model B ($\dot{N}^{4\pi,B}_{\rm TDE}/10^3$) for all source redshifts (fifth column) and $0 < z < 3$ (sixth column).

Model	Flux limit	$\frac{\dot{N}^{4\pi,A}_{\rm TDE}}{10^3}$ All	$\frac{\dot{N}^{4\pi,A}_{\rm TDE}}{10^3}$ $z < 3$	$\frac{\dot{N}^{4\pi,B}_{\rm TDE}}{10^3}$ All	$\frac{\dot{N}^{4\pi,B}_{\rm TDE}}{10^3}$ $z < 3$
$f_{\rm occ} = 1$	BAT	0.93	0.62	4.3	3.9
	50 ×BAT	11	9	47	24
$f_{\rm occ} = 0$	BAT	0.27	0.25	1.3	0.99
	50 ×BAT	2.4	1.5	4.6	3.6

Table 3. For each model, we show the fraction of TDEs sourced by binaries at each flux limit for Model A ($F^{\rm BAT}_{\rm Bin,A}$, column 3) and Model B ($F^{\rm BAT}_{\rm Bin,B}$, column 4).

Model	Flux limit	$F^{\rm BAT}_{\rm Bin,A}$	$F^{\rm BAT}_{\rm Bin,B}$
$f_{\rm occ} = 1$	*Swift*	64 per cent	4.6 per cent
	50 × *Swift*	22 per cent	3.6 per cent
	Ideal	0.72 per cent	0.72 per cent
$f_{\rm occ} = 0$	*Swift*	1.3 per cent	0.05 per cent
	50 × *Swift*	0.5 per cent	0.09 per cent
	Ideal	0.17 per cent	0.17 per cent

the occupation fraction of IMBHs, could be verified observationally by analysing the variability of each event and comparing to the models available in the literature (Liu et al. 2009, 2014; Coughlin et al. 2016; Ricarte et al. 2016).

Another observational mode is when the telescope takes a snapshot of the same part of the sky with a long exposure (integration time). The snapshot mode allows to probe a smaller portion of the sky with greater sensitivity than is done in the survey mode. A telescope with integration time $t_{\rm int}$ will measure the following number of new events per frame (Woods & Loeb 1998)

$$N_{\rm TDE}^{S>S_{\rm lim}} = f_{\rm sky} \int_0^{z_{\rm max}} \int_{S_{2-10}>S_{\rm lim}} \frac{\dot{N}_{\rm TDE}}{(1+z)} \frac{{\rm d}V}{{\rm d}z} {\rm d}z {\rm d}S \times \min\left[t_{\rm int}, t_{\rm dur}(1+z)\right], \quad (14)$$

where $t_{\rm dur}$ is the time during which the event is above the sensitivity limit of the telescope, and $f_{\rm sky}$ is the sky fraction covered by the telescope. The typical integration time of a telescope such as XRT, $\sim 10^4$ s, is much shorter than the typical duration of a TDE event ($\sim 10^6$ s, fall-back time), and thus, $t_{\rm dur}$ can be ignored compared to $t_{\rm int}$. To complete our discussion of *Swift* capabilities in detecting TDEs, we show in the blue coordinate system of Fig. 5 the expected number of events per typical exposure time of 10^4 s in a field of view of 1 deg^2 assuming that all events shine at their peak luminosity. The number counts expected for the XRT sensitivity are much smaller than unity (see Fig. 5 for details) meaning that XRT is good for follow-up missions but not to detect new TDEs, unless larger integration times are chosen.

The snapshot regime also applies to telescopes such as *Chandra* that observe one patch of the sky (15×15 deg^2 in the case of *Chandra*) for a long time (more than 10^6 s). The next-generation upgrade of *Chandra*, called the *X-ray Surveyor*, is proposed to have $\sim$30 times bigger collecting area than *Chandra* and, therefore, better sensitivity (Weisskopf et al. 2015). A small fraction of point sources in each snapshot taken by *Chandra* (or the future *X-ray Surveyor*) could be TDEs and mistakenly identified as steady sources because of their long decay times. To single them out, a succession of snapshots of the same field should be taken within a time interval longer than a year. Because of the very long integration time of deep field survey, the TDE flux would decline below the flux limit in the course of the observation. To estimate the expected number of hidden TDEs in a *Chandra* deep field, we use equation (14) and assume that the light curve of each source fades according to equation (9). Fig. 6 shows the increment in the observed number counts per one snapshot as the telescope sensitivity limit improves. The number counts of SMBHs saturate at sensitivities $S_{\rm lim} \sim 10^{-17}$–$10^{-16}$ erg s^{-1}, while the number counts of MBHs keep rising with decreasing $S_{\rm lim}$. Comparing observed TDE luminosity function to the 6σ detection level ($\sim 2.4 \times 10^{-16}$ erg cm^{-2} s^{-1} in 10^6 s), we estimate number of TDEs in one *Chandra* deep field of 15×15 arcmin^2 to be 0.3–0.7 for SMBHs and 0.7–4 for MBHs. For a future mission such as the *X-ray Surveyor*, TDE number counts remain $\sim$0.7 for SMBHs, while they evolve to $\sim$6–20 for MBHs. Therefore, non-detection of TDEs in a deep field would be a strong evidence for either a low occupation fraction of IMBHs, e.g. if they are kicked out of their parent haloes as a result of mergers (O'Leary & Loeb 2012) or a direct collapse scenario, e.g. works by Bromm & Loeb (2003), Ryu et al. (2016), Latif & Ferrara (2016) and Chon et al. (2016).

Interestingly, current surveys with *Chandra* and *XMM–Newton* find an exponential decline in the space density of luminous AGNs at $z > 3$ (Brandt & Vito 2017) suggesting that MBHs might not exist at higher redshifts. As Table 2 shows, in our Models A & B for

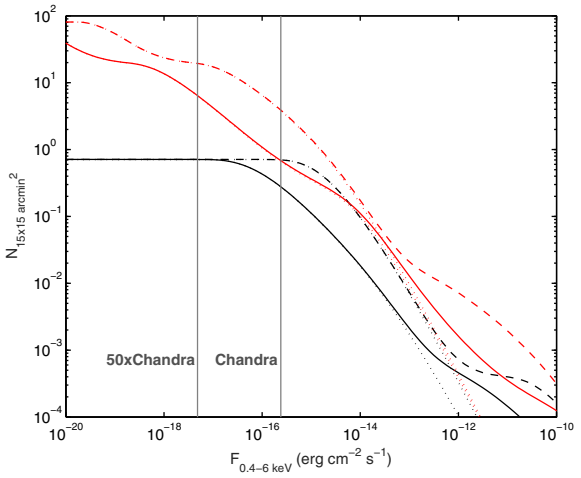

Figure 6. Number counts per one deep exposure with a telescope such as the *Chandra X-ray Observatory*. The grey vertical lines show 6σ sensitivity of 2.4×10^{-16} erg s^{-1} and a 50 times better sensitivity, for an integration time of 4 Ms.

current BAT sensitivity, 67 per cent & 92 per cent of all observable TDEs are expected to originate at $z < 3$ for MBHs (and 94 per cent & 77 per cent for SMBHs); while for a 50 times more sensitive telescope, the corresponding numbers for MBHs are 83 per cent & 52 per cent (66 per cent & 78 per cent for SMBHs). For *Chandra*, the corresponding numbers are 68 per cent & 70 per cent ($f_{\rm occ} = 1$) and 83 per cent & 50 per cent ($f_{\rm occ} = 0$), while for its successor 52 per cent & 35 per cent for MBHs and 49 per cent for SMBHs.

The maximal redshift out to which TDEs can be detected depends on the telescope sensitivity. Fig. 7 shows the TDE rates in the survey mode (BAT, left) and number of TDEs observed per snapshot (*Chandra*, right) for several choices of $S_{\rm lim}$ including present-day instrument, a 50 $\times$ more sensitive telescope and an ideal detector that identifies both jetted and non-jetted TDE accounting only for redshifts $z > z_{\rm min}$. In other words, for each telescope sensitivity, we only account for the events that originate at $z_{\rm min}$ or above. As we probe higher redshifts, the expected number of sources drops because there are no sufficiently massive haloes to source sufficiently bright flares. The left-hand panel of Fig. 6 focuses on a BAT-like survey that is primarily sensitive to bright (mainly jetted) events. It is evident that if TDEs do not source jets, prospects for observations with BAT would not be as bright, and TDEs would be observable only out to $z \sim 0.1$ with BAT and out to $z = 0.4$ with a 50 times more sensitive telescope than BAT. The redshifts at which number of observed TDE per year drops by a factor of 2 ($z_{50\ \text{per cent}}^{\rm BAT}$) and 10 ($z_{10\ \text{per cent}}^{\rm BAT}$) are listed in Table 4 for all models under consideration. Note that in some cases, $z_{50\ \text{per cent}}^{\rm BAT}$ does not change monotonically as a function of the sensitivity. This is because the non-jetted events become unobservable despite being more numerous while few jetted events are seen out to greater distances. The right-hand panel of Fig. 7 focuses on a *Chandra*-like instrument that has more sensitivity and integration time but a smaller field of view than *Swift*. If the IMBHs occupancy is high, 50 per cent of events observed by *Chandra* would originate from $z \lesssim 2$ (and $z \lesssim$ 2–4 if observed by *Chandra* successors with the uncertainty arising from our luminosity modelling). For completeness, we also consider XRT. As expected, XRT is mainly sensitive to non-jetted TDEs and 50 per cent of TDEs that can be observed by XRT are predicted to originate from $z \lesssim$ 0.4–1. This is broadly consistent

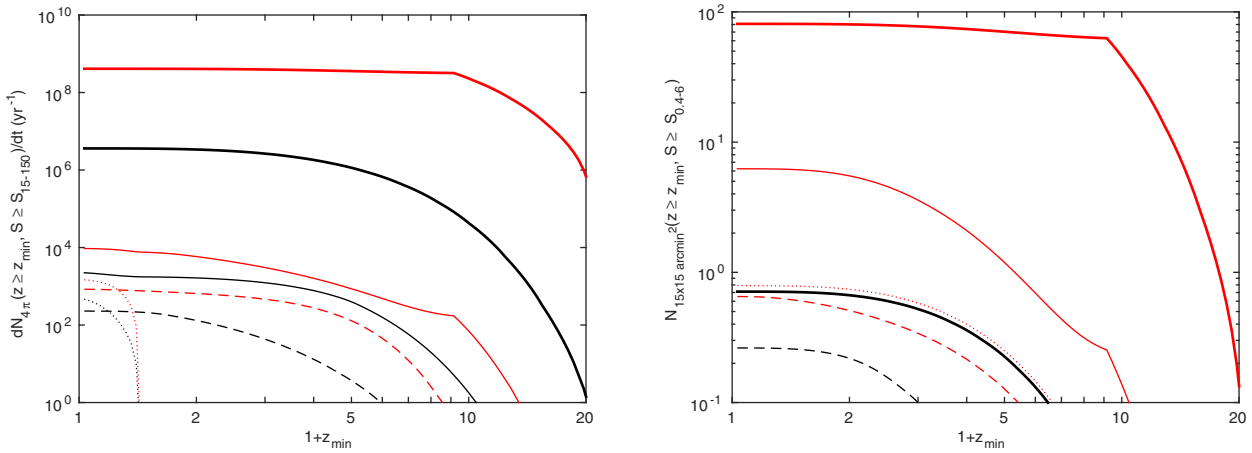

Figure 7. TDE number counts originating from $z \geq z_{\rm min}$ for SMBHs (black) and MBHs (red) in Model A. In all cases, we account for the contribution of both single and binary black holes, as well as for 10 per cent jetted events (which are visible out to higher redshifts). We also show a non-jetted population observed with a 50 times more sensitive telescope than present (dotted). Left: hard X-ray counts observed in a survey mode over the whole sky per year for a telescope with sensitivity of $S_{\rm lim}$ for BAT (dashed), future 50 ×BAT (thin solid) and an infinitely sensitive survey (thick solid). Right: soft X-ray counts observed in a snapshot mode over 15×15 arcmin^2 field for a telescope with sensitivity for *Chandra* (dashed), 50 ×*Chandra* (thin solid) and an ideal future survey that finds all sources (thick solid).

Table 4. The redshift $z_{\rm min}$ so that 50 per cent (columns 3 and 5 for Models A and B, respectively), and 10 per cent (columns 4 and 6) of observed BAT TDEs arrive from $z > z_{\rm min}$.

Model	Flux limit	$z^{\rm BAT}_{50\ \text{per cent,A}}$	$z^{\rm BAT}_{10\ \text{per cent,A}}$	$z^{\rm BAT}_{50\ \text{per cent,B}}$	$z^{\rm BAT}_{10\ \text{per cent,B}}$
$f_{\rm occ} = 1$	*Swift*	2.2	4.4	1.2	2.6
	50 × *Swift*	1.3	3.8	2.8	5.3
	Ideal	9.0	12.6	9.0	12.6
$f_{\rm occ} = 0$	*Swift*	1.1	2.5	2.0	3.2
	50 × *Swift*	2.2	4.6	0.2	4.8
	Ideal	3.0	5.9	3.0	5.9

with the current sample (Komossa 2015) in which all non-jetted TDEs are identified to be at $z \sim 0.405$ while the rare jetted events are observed at $z = 0.353$, 0.89 and 1.186.

The signature of reionization, due to the evolving $M_{\rm BH,min}$ in star-forming haloes, is evident in MBH cases and manifests itself as a cusp around $z_{\rm re} = 8.8$. Because we assume instantaneous reionization, the feature is sharp. In a more realistic case of gradual reionization, the signature is expected to show as a mild enhancement of the TDE rates at $z \gtrsim z_{\rm re}$.

5 CONCLUSIONS

Current observations pose only poor constraints on MBH growth at high redshifts as well as on the occupation fraction of IMBHs. Flares from TDEs could reveal the population of otherwise dormant black holes allowing us to constrain the contribution of IMBHs. In this paper, we have considered evolution of the observable TDE number counts with X-ray telescopes including predictions for future missions. Our discussion of the black hole mass distribution included a model with $f_{\rm occ} = 1$ (all star-forming haloes are occupied by black holes) and $f_{\rm occ} = 0$ (only heavy haloes host black holes of $M_{\rm BH} > 10^6\,{\rm M}_\odot$). These two scenarios provide upper and lower limits for the expected number counts, respectively. In addition, we considered two different prescriptions for the TDE luminosity: (i) Eddington luminosity and (ii) luminosity proportional to the accretion rate with an upper limit of $300\,L_{\rm Edd}$ in agreement with observations and numerical simulations. Finally, we assume that 10 per cent of TDEs trigger relativistic jets.

Even though current TDE observations suggest that the occupation fraction of IMBHs is very low with the majority of TDEs being produced by black holes of masses $\sim 10^6$–$10^8\,{\rm M}_\odot$, the results are far from being conclusive. Our study offers new ways to constrain the occupation fraction of IMBHs at different cosmological redshifts, and our main conclusions are as follows.

(i) We show that jetted TDEs can be observed out to high redshifts and offer a unique probe of the occupancy of IMBHs. Earlier works have demonstrated that TDE rates in merging systems are enhanced due to gravitational interactions of stars with binary black holes. Using this result, we find that the higher is the occupation fraction of IMBHs the stronger is the impact of binaries on the total observed TDE rates. This is because with high IMBH occupation, there are enough progenitors to form binary systems.

(ii) We show that TDEs sourced by binary black holes dominate the bright end of the X-ray luminosity function if the occupation fraction of IMBHs is high. The shape of the TDE X-ray luminosity function is expected to show a unique signature of IMBHs in the form of two additional 'knees', compared to the case with low IMBH occupation. These features arise from the jetted and non-jetted contribution of black hole binaries and are independent of our luminosity prescription. Therefore, for a complete TDE sample, the shape of the luminosity function could be used to set an upper limit on the occupation fraction of IMBHs. Our results imply

that, if $f_{\rm occ} = 1$, the brightest events detected by BAT could be associated with massive binary black holes, and in this case the X-ray luminosity of TDE flares is expected to have excess of variability due to the binary interaction in addition to the typical power-law decay.

(iii) The fraction of observable TDE that are generated by binaries depends on the luminosity prescription as well as on the sensitivity of the telescope. With current X-ray telescopes, we expect to see >2 per cent and up to 64 per cent of TDEs produced by binary black holes if the occupation fraction of IMBHs is high; while the fraction is at most 1.3 per cent if the occupation fraction of IMBHs is low. Since dimmer events are mainly contributed by single black holes, the binary fraction drops with the telescope sensitivity.

(iv) Detection of TDEs in deep field observations by *Chandra* and future missions would provide a smoking gun signature of IMBHs. We find that in the case when only SMBHs contribute, TDEs are not expected in *Chandra* deep fields; while if the IMBHs occupation fraction is high, some point sources in the archival data of X-ray deep field surveys may be TDEs. To identify such events, one should compare two images of the same deep field separated by an interval of at least a year. Non-detection of TDEs from high redshifts can set upper limits on the occupation fraction of IMBHs and constrain direct collapse scenarios of SMBH formation, e.g. works by Bromm & Loeb (2003), Ryu et al. (2016), Latif & Ferrara (2016) and Chon et al. (2016).

(v) Increasing sensitivity of X-ray telescopes by a factor of 50 comparing to current instruments will increase the expected number counts by a factor of 4–10 for a BAT-like mission and a factor of 20–40 for an XRT-like mission with 1 ks integration time. For a deep field survey, the improvement strongly depends on the occupation fraction of IMBHs. Current sensitivity is enough to resolve most TDEs if $f_{\rm occ} = 0$, and, therefore, improvement in sensitivity would not yield new events in this case. However, if $f_{\rm occ} = 1$, improving the sensitivity by a factor of 50 would increase the number of TDEs per snapshot by a factor of 5–10.

Comparing our model to existing observations, a low occupation fraction is suggested (see also Stone & Metzger 2016). However, observations are far from being conclusive and it is still unclear why TDEs sourced by IMBHs with masses below $10^6\,{\rm M}_\odot$ are not observed. Several possible explanations can follow: IMBHs are kicked out of their dark matter haloes as a result of mergers (O'Leary & Loeb 2012), SMBHs are formed from massive seeds in massive haloes, observational selection effects exclude TDEs around IMBHs, the assumption of an isothermal density distribution is less suitable for smaller galaxies or low-mass systems are more sensitive to AGN feedback that expels gas from halo and limits star formation leading to inefficient replenishing of the loss cone.

If $f_{\rm occ}$ is high at low black hole masses and IMBH binaries indeed play a role in sourcing TDEs, these binaries would also produce gravitational waves on their approach to coalescence. eLISA should be sensitive to MBH binaries over a wide range of total masses and mass ratios, e.g. systems with total mass $\gtrsim 10^5\,{\rm M}_\odot$ and mass ratios of $\gtrsim$0.1 will yield signal-to-noise ratio of >20 out to $z = 4$ (Amaro-Seoane et al. 2012). Therefore, in the future one could use a cross-correlation between the stochastic gravitational wave background and the spatial distribution of brightest TDEs to constrain the role of IMBHs in TDE production. If the two quantities correlate, IMBHs must make a significant contribution to TDEs.

In addition to the X-ray observations discussed here, jetted TDEs may also be bright in the radio band (Levan et al. 2011; Zauderer et al. 2011). Snapshot rates of jetted TDEs in the radio band have been computed by van Velzen et al. (2011), and prospects for the detection of jetted TDEs by the Square Kilometer Array out to $z \sim 2$ as well as the synergy between radio and X-ray observations was discussed (Donnarumma & Rossi 2015; Donnarumma et al. 2015; Rossi et al. 2015). Compared to X-rays, the peak emissivity of Sw1644+57 appeared 100 d after the BAT trigger and the Lorentz factor of radio jet was found to be $\Gamma \sim 2$, much lower than what was observed in X-rays right after detection ($\Gamma \sim 10$). In addition, Yang et al. (2016) have directly measured the apparent speed of the radio jet formed by Sw1644+57 to be less than $0.3c$ (when averaged over 3 yr) using Very Long Baseline Interferometry (VLBI). Similar VLBI measurements for nearby TDEs may be useful in constraining the radio jets formed by other TDEs. With these data in hand, predictions for the TDE rates observed by the SKA and their correlation with X-ray observations could be improved.

Tidal disruptions occurring at high redshifts can reveal the seeds of quasars. In this paper, we have assumed that the high-redshift population resembles that of today; however, its properties might evolve with redshift. In particular, simulations show that first stars were much more massive (up to $10^3\,{\rm M}_\odot$) than present-day stars and could serve as an additional population of seeds. Star formation in high-redshift, low-mass haloes strongly depends on feedback processes such as photoheating feedback, as well as AGN and supernovae feedback. The evolution of the TDE number counts with redshift could serve as a smoking gun for these processes.

ACKNOWLEDGEMENTS

We thank J. Guillochon for helpful comments on the manuscript. We also thank J. Guillochon, A. Sądowski, Y.-F. Jiang and A. Siemiginowska for useful discussions. This work was supported in part by Harvard's Black Hole Initiative, which is supported by a grant from the John Templeton Foundation.

REFERENCES

Amaro-Seoane P. et al., 2012, Class. Quantum Gravity, 29, 124016
Arcavi I. et al., 2014, ApJ, 793, 38
Bade N., Komossa S., Dahlem M., 1996, A&A, 309, L35
Baldassare V. F., Reines A. E., Gallo E., Greene J. E., 2015, ApJ, 809, 14
Baldassare V. F., Reines A. E., Gallo E., Greene J. E., 2017, ApJ, 836, 20
Bañados E. et al., 2015, ApJ, 804, 118
Bar-Or B., Alexander T., 2016, ApJ, 820, 129
Barkana R., 2016, Phys. Rep., 645, 1
Barthelmy S. D. et al., 2005, Space Sci. Rev., 120, 143
Bloom J. S. et al., 2011, Science, 33, 203
Bower G. C., Metzger B. D., Cenko S. B., Silverman J. M., Bloom J. S., 2013, ApJ, 763, 84
Brandt W. N., Vito F., 2017, Astron. Nachr., 338, 241
Bromm V., Loeb A., 2003, ApJ, 596, 34
Brown G. C., Levan A. J., Stanway E. R., Tanvir N. R., Cenko S. B., Berger E., Chornock R., Cucchiaria A., 2015, MNRAS, 452, 4297
Burrows D. N. et al., 2011, Nature, 476, 421
Carter B., Luminet J.-P., 1983, A&A, 121, 97
Cenko S. B. et al., 2012, ApJ, 753, 77
Chen X., Madau P., Sesana A., Liu F. K., 2009, ApJ, 697, 149
Chen X., Sesana A., Madau P., Liu F. K., 2011, ApJ, 729, 13
Chon S., Hirano S., Hosokawa T., Yoshida N., 2016, ApJ, 832, 134
Chornock R. et al., 2014, ApJ, 780, 44
Cohen A., Fialkov A., Barkana R., 2016, MNRAS, 459, 90
Cohn H., Kulsrud R. M., 1978, ApJ, 226, 1087
Colpi M., 2014, Space Sci. Rev., 183, 189
Coughlin E. R., Armitage P. J., Nixon C., Begelman M. C., MNRAS, 465, 3840

Dai L., McKinney J. C., Miller M. C., 2015, ApJ, 812, L39
Donley J. L., Brandt W. N., Eracleous M., Boller Th., 2002, AJ, 124, 1308
Donnarumma I., Rossi E. M., 2015, ApJ, 2015, 803, 36
Donnarumma I., Rossi E. M., Fender R., Komossa S., Paragi Z., Van Velzen S., Prandoni I., 2015, Proc. Sci., SKA as a powerful hunter of jetted Tidal Disruption Events. SISSA, Trieste, PoS(AASKA14)054
Esquej P. et al., 2008, A&A, 489, 543
Evans C. R., Kochaneck C. S., 1989, ApJ, 346, L13
Fakhouri O., Ma C.-P., Boylan-Kolchin M., 2010, MNRAS, 406, 2267
Farrell S. A., Webb N. A., Barret D., Godet O., Rodrigues J. M., 2009, Nature, 460, 73
Frank J., Rees M. J., 1976, MNRAS, 176, 633
Generozov A., Mimica P., Metzger B. D., Stone N. C., Giannios D., Aloy M. A., 2017, MNRAS, 464, 2481
Gezari S. et al., 2006, ApJ, 653, L25
Gezari S. et al., 2008, ApJ, 676, 944
Gezari S. et al., 2009, ApJ, 698, 1367
Gezari S. et al., 2012, Nature, 485, 217
Ghisellini G., Della Ceca R., Volonteri M., Ghirlanda G., Tavecchio F., 2010, MNRAS, 405, 387
Graham A., 2016, Astrophysics and Space Science Library, Vol. 418, Galactic Bulges. Springer, Berlin, p. 263
Greene J. E., 2012, Nat. Commun., 3, 1304
Greene J. E., Ho L. C., 2007, ApJ, 667, 131
Guillochon J., Loeb A., 2015, ApJ, 806, 124
Guillochon J., McCourt M., 2017, ApJ, 834, L19
Guillochon J., Ramirez-Ruiz E., 2013, ApJ, 767, 25
Guillochon J., McCourt M., Chen X., Johnson M. D., Berger E., 2016, ApJ, 822, 48
Gultekin K. et al., 2009, ApJ, 698, 198
Hayasaki K., Stone N., Loeb A., 2016, MNRAS, 461, 3760
Hill J. G., 1975, Nature, 254, 295
Hirano S., Hosokawa T., Yoshida N., Omukai K., Yorke H. W., 2015, MNRAS, 448, 568
Holoien T. W.-S. et al., 2014, MNRAS, 445, 3263
Hopman C., Alexander T., 2006, ApJ, 645, 1152
Inayoshi K., Haiman Z., Ostriker J. P., 2016, MNRAS, 459, 3738
Ivanov P. B., Polnarev A. G., Saha P., 2005, MNRAS, 358, 1361
Jiang L., Fan X., Ivezić Ž., Richards G. T., Schneider D. P., Strauss M. A., Kelly B. C., 2007, ApJ, 656, 680
Jiang Y.-F., Stone J. M., Davis S. W., 2014, ApJ, 796, 106
Kara E., Miller J. M., Reynolds C., Dai L., 2016, Nature, 535, 388
Kawamuro T., Ueda Y., Shidatsu M., Hori T., Kawai N., Negoro H., Mihara T., 2016, PASJ, 68, 58
Khabibullin I., Sazonov S., 2014, MNRAS, 444, 1041
Komossa S., 2015, J. High Energy Astrophys., 7, 148
Komossa S., Bade N., 1999, A&A, 343, 775
Kormendy J., Ho L. C., 2013, ARA&A, 51, 511
Kormendy J., Richstone D., 1995, ARA&A, 33, 581
Lacy J. H., Townes C. H., Hollenbach D. J., 1982, ApJ, 262, 120
Latif M., Ferrara A., 2016, Publ. Astron. Soc. Aust., 33, e051
Lemons S. M., Reines A. E., Plotkin R. M., Gallo E., Greene J. E., 2015, ApJ, 805, 12
Levan A. J., Tanvir N. R., Cenko S. B., 2011, Science, 33, 199
Lezhnin K., Vasiliev E., 2015, ApJ, 808, L5
Lezhnin K., Vasiliev E., 2016, ApJ, 831, 84
Li G., Naoz S., Kocsis B., Loeb A., 2015, MNRAS, 451, 1341
Li S., Liu F. K., Berczik P., Spurzem R., 2017, ApJ, 834, 195
Lightman A. P., Shapiro S. L., 1977, ApJ, 211 244
Liu F. K., Chen X., 2013, ApJ, 767, 18
Liu F. K., Li S., Chen X., 2009, ApJ, 706, L133
Liu F. K., Li S., Komossa S., 2014, ApJ, 786, 103
Loeb A., Furlanetto S., 2013, The First Galaxies in the Universe. Princeton Univ. Press, Princeton, NJ
Luo B., Brandt W. N., Steffen A. T., Bauer F. E., 2008, ApJ, 674, 122
McConnell N. J., Ma C.-P., 2013, ApJ, 764, 184
Machacek M. E., Bryan G. L., Abel T., 2001, ApJ, 548, 509
McKinney J. C., Tchekhovskoy A. Sądowski A., Narayan R., 2014, MNRAS, 441, 3177
McKinney J. C., Dai L., Avara M. J., 2015, MNRAS, 454, 6
MacLeod M., Goldstein J., Ramirez-Ruiz E., Guillochon J., Samsing J., 2014, ApJ, 794, 9
Magorrian J., Tremaine S., 1999, MNRAS, 309, 447
Magorrian J. et al., 1998, AJ, 115, 2285
Maksym W. P., Ulmer M. P., Eracleous M., 2010, ApJ, 722, 1035
Merritt D., 2015, ApJ, 804, 128
Merritt D., Poon M.-Y., 2004, ApJ, 606, 788
Merritt D., Wang J., 2005, ApJ, 621, L101
Metzger B. D., Giannios D., Mimica P., 2012, MNRAS, 420, 3528
Miller B. P., Gallo E., Greene J. E., Kelly B. C., Treu T., Woo J.-H., Baldassare V., 2015, ApJ, 799, 98
Mimica P., Giannios D., Metzger B. D., Aloy M. A., 2015, MNRAS, 450, 2824
Moran E. C., Shahinyan K., Sugarman H. R., Velez D. O., Eracleous M., 2014, AJ, 148, 136
O'Leary R. M., Loeb A., 2012, MNRAS, 421, 2737
Pasham D. R. et al., 2015, ApJ, 805, 68
Perets H., Hopman C., Alexander T., 2006, ApJ, 656, 709
Phinney E. S., 1989, Nature, 340, 595
Piran T., Sądowski A., Tchekhovskoy A., 2015, MNRAS, 453, 157
Planck Collaboration XLVII, 2016, A&A, 596, A108
Rauch K., Tremaine S., 1996, New Astron., 1, 149
Rees M. J., 1988, Nature, 333, 523
Rees M. J., 1990, Science, 247, 817
Reines A. E., Greene J. E., Geha M., 2013, ApJ, 775, 116
Ricarte A., Natarajan P., Dai L., Coppi P., 2016, MNRAS, 458, 1712
Rossi E. M., Donnarumma I., Fender R., Jonker P., Komossa S., Paragi Z., Prandoni I., Zampieri L., 2015, preprint (arXiv:1501.02774)
Roth N., Kasen D., Guillochon J., Ramirez-Ruiz E., 2016, ApJ, 827, 3
Ryu T., Tanaka T. L., Perna R., Haiman Z., 2016, MNRAS, 460, 4122
Saglia R. P. et al., 2016, ApJ, 818, 47
Sakurai Y., Inayoshi K., Haiman Z., 2016, MNRAS, 461, 4496
Saxton R. D., Read A. M., Esquej P., Komossa S., Dougherty S., Rodriguez-Pascual P., Barrado D., 2012, A&A, 541, 106
Saxton R. D., Read A. M., Komossa S., Lira P., Alexander K. D., Wieringa M. H., 2017, A&A, 598, A29
Sheth R. K., Tormen G., 1999, MNRAS, 308, 119
Shiokawa H., Krolik J. H., Cheng R. M., Piran T., Noble S. C., 2015, ApJ, 804, 85
Sobacchi E., Mesinger A., 2013, MNRAS, 432, 3340
Stern D. et al., 2004, ApJ, 612, 690
Stone C. N., Metzger B. D., 2016, MNRAS, 455, 859
Stone C. N., Sari R., Loeb A., 2013, MNRAS, 435, 1809
Sądowski A., Narayan R., 2015, MNRAS, 453, 3213
Sądowski A., Narayan R., Tchekhovskoy A., Abarca D., Zhu Y., McKinney J. C., 2015, MNRAS, 447, 49
Tchekhovskoy A., Metzger B. D., Giannios D., Kelley L. Z., 2014, MNRAS, 437, 2744
Tegmark M., Silk J., Rees M. J., Blanchard A., Abel T., Palla F., 1997, ApJ, 474, 1
Thomas J., Ma C.-P., McConnell N. J., Greene J. E., Blakeslee J. P., Janish R., 2016, Nature, 532, 340
van Velzen S., Farrar G. R., 2014, ApJ, 792, 53
van Velzen S. et al., 2011, ApJ, 741, 73
van Velzen S., Frail D. A., Körding E., Falcke H., 2013, A&A, 552, A5
Vasiliev E., 2014, Class. Quantum Gravity, 31, 244002
Vasiliev E., Merritt D., 2013, ApJ, 774, 87
Vasudevan R. V., Fabian A. C., 2007, MNRAS, 381, 1235
Villforth C. et al., 2017, MNRAS, 466, 812
Vinko J. et al., 2015, ApJ, 798, 12
Wang J., Merritt D., 2004, ApJ, 600, 149
Wang T., Zhou H.-Y., Komossa S., Wang H.-Y., Yuan W., Yang C., 2012, ApJ, 749, 115
Wegg C., Bode J. N., 2011, ApJ, 738, 8

Weisskopf M. C., Gaskin J., Tananbaum H., Vikhlinin A., 2015, in Hudec R., Pina L., eds, Proc. SPIE Conf. Ser. Vol. 9510, EUV and X-ray Optics: Synergy between Laboratory and Space IV. SPIE, Bellingham
Woods E., Loeb A., 1998, ApJ, 508, 760
Wyithe S., Loeb A., 2013, MNRAS, 428, 2741
Yang J., Paragi Z., van der Horst A. J., Gurvits L. I., Campbell R. M., Giannios D., An T., Komossa S., 2016, MNRAS, 462, L66
Yuan W., Zhou H., Dou L., Dong X.-B., Fan X., Wang T.-G., 2014, ApJ, 782, 55
Zauderer B. A. et al., 2011, Nature, 476, 425

This paper has been typeset from a TEX/LATEX file prepared by the author.